Geophysical Research Letters

RESEARCH LETTER
10.1029/2022GL102550

Controls on Wintertime Ventilation in Southern Drake Passage

Lilian A. Dove[1], Giuliana A. Viglione[1,2], Andrew F. Thompson[1], M. Mar Flexas[1], Taylor R. Cason[3], and Janet Sprintall[4]

[1]Environmental Science and Engineering, California Institute of Technology, Pasadena, CA, USA, [2]Carbon Brief, London, UK, [3]University of California Los Angeles, Los Angeles, CA, USA, [4]Scripps Institution of Oceanography, University of California San Diego, La Jolla, CA, USA

Abstract Drake Passage is a key region for transport between the surface and interior ocean, but a mechanistic understanding of this exchange remains immature. Here, we present wintertime, submesoscale-resolving hydrographic transects spanning the southern boundary of the Antarctic Circumpolar Current and the Polar Front (PF). Despite the strong surface wind and buoyancy forcing, a freshwater lens suppresses surface-interior exchange south of the PF; ventilation is instead localized to the PF. Multiple lines of the analysis suggest submesoscale processes contribute to ventilation at the PF, including small-scale, O(10 km), frontal structure in water mass properties below the mixed layer and modulation of a surface eddy diffusivity at sub-50 km scales. These results show that ventilation is sensitive to both submesoscale properties near fronts and non-local processes, for example, sea-ice melt, that set stratification and mixed layer properties. This highlights the need for adaptive observing strategies to constrain Southern Ocean heat and carbon budgets.

Plain Language Summary Drake Passage is a region of the Southern Ocean between the southern tip of South America and the Antarctic Peninsula. Due to its relative accessibility as compared to the rest of the polar ocean, it is the most frequently occupied region of the Southern Ocean. Most occupations by ships in Drake Passage acquire measurements at 20–100 km spacing or "mesoscale" resolution. Here, we present data collected by piloted robotic underwater vehicles that sampled across the southern section of Drake Passage with submesoscale, or 1–10 km, resolution in wintertime. These novel observations indicate that while the southernmost region of Drake Passage is strongly stratified in density, the Polar Front (PF), one of the major dynamical features of the Southern Ocean, is more weakly stratified. The reduced stratification at the PF presents a pathway for the localized exchange of water between the surface and interior ocean. In addition, this study finds that the PF is eddy-suppressing, meaning that the mean flow of the PF can transport oceanic properties away before they can be stirred. These findings have implications for the estimation of carbon fluxes between the atmosphere and the Southern Ocean, a vital part of the climate system.

Lilian A. Dove and Giuliana A. Viglione contributed equally to this work.

Key Points:

- High-resolution hydrographic sections across the Drake Passage provide insight into spatial variability in surface-interior exchange
- Wintertime observations suggest ventilation is spatially localized to the Polar Front and influenced by submesoscale processes
- A mixing length estimate shows modulation at submesoscales and mixing suppression in the upper layers of the Polar Front

Supporting Information:

Supporting Information may be found in the online version of this article.

Correspondence to:

L. A. Dove,
dove@caltech.edu

Citation:

Dove, L. A., Viglione, G. A., Thompson, A. F., Flexas, M. M., Cason, T. R., & Sprintall, J. (2023). Controls on wintertime ventilation in southern Drake Passage. *Geophysical Research Letters*, *50*, e2022GL102550. https://doi.org/10.1029/2022GL102550

Received 15 DEC 2022
Accepted 13 FEB 2023

1. Introduction

More than 40% of anthropogenic carbon in the ocean has been taken up south of 40°S, making the Southern Ocean one of the primary regulators of global climate (Frölicher et al., 2015; Sallée et al., 2012). The position at which isopycnals outcrop at the surface in the Southern Ocean has a leading-order impact on climate as this determines the structure and strength of the overturning circulation, as well as the magnitude of air–sea fluxes, which together control ventilation rates of surface waters (Abernathey et al., 2016; Ferrari et al., 2014; Pellichero et al., 2018; Speer et al., 2000). Following Morrison et al. (2022), we refer to "ventilation" as any process, or combination of processes, that transfers surface waters and tracers into the pycnocline. Drake Passage is a key region for the formation of mode waters (Close et al., 2013; Naveira Garabato et al., 2009; Sallée et al., 2010) and the ventilation of carbon (Sallée et al., 2012). Wintertime measurements of pCO_2 have, until recently, only been collected in Drake Passage, and thus processes governing the exchange of carbon with the atmosphere here have had an outsized influence on the interpretation of carbon cycling across the Southern Ocean (Takahashi et al., 2009, 2012). This sampling bias may contribute to differences between estimates of air–sea CO_2 fluxes from climatology, autonomous platforms (Gray et al., 2018; Sutton et al., 2021), atmospheric inversion (Landschützer et al., 2015), and aircraft observations (Long et al., 2021).

The Antarctic Circumpolar Current (ACC) is dominated by several major fronts that result in sharp transitions of water properties, with these fronts delimiting boundaries between different water masses (Chapman et al., 2020; Orsi et al., 1995). Frontal jets contribute the majority of the ACC's zonal transport, but also act as barriers to

mixing and cross-front exchange by reducing the efficiency at which mesoscale eddies can stir tracers (Ferrari & Nikurashin, 2010; Klocker et al., 2012; Naveira Garabato et al., 2011; Thompson & Sallée, 2012). The ACC's fronts additionally connect the interior ocean with the atmosphere through both upwelling of deep waters and the subduction of surface waters. In particular, the Antarctic Circumpolar Current's Polar Front (PF) is a key location where the formation of intermediate and mode waters occurs, impacting carbon and heat exchange with the atmosphere (Morrison et al., 2022; Stukel et al., 2017). Previous work has typically not resolved small-scale processes that influence both ventilation and eddy mixing at strong fronts.

Mesoscale stirring and submesoscale motions in the ocean surface boundary layer can significantly alter upper-ocean stratification and exchange between the mixed layer and the thermocline (Klein & Lapeyre, 2009). Coherent mesoscale eddies impact tracer structure at horizontal scales of O(10–100 km). Meanwhile, submesoscale motions are characterized by length scales of O(1–10 km) and Rossby numbers of O(1), dynamical regimes where rotation and inertial forces are of comparable importance. Process-based modeling studies of the Southern Ocean have suggested that submesoscale motions play a critical role in determining vertical fluxes of heat (Rosso et al., 2014), mixed layer depths (Bachman et al., 2017), and exchange across the base of the mixed layer (Balwada et al., 2018), underlining the need to accurately represent these dynamics in global climate models. Numerical studies have also found a heterogeneous distribution of submesoscale characteristics across the Southern Ocean with recent observations highlighting that these dynamical transitions are often abrupt and intermittent (Adams et al., 2017; Dove et al., 2021; Giddy et al., 2021; du Plessis et al., 2017, 2019; Viglione et al., 2018). Estimates of Southern Ocean carbon subduction based on mesoscale and coarser observations (Sallée et al., 2012) have highlighted spatial variability in the ACC at O(1,000 km) scales; our analysis here suggests that significant variations in these climatically relevant air–sea exchange and ventilation properties occur on much finer scales in localized regions.

We present a unique, high-resolution hydrographic data set from Drake Passage, acquired by an autonomous ocean glider during the austral winter 2016, that permits assessment of how variability at scales smaller than mesoscale impact ventilation and mixing rates. This study contributes to growing evidence that submesoscale dynamics are spatially and temporally heterogeneous in the Southern Ocean, responding not only to local, mesoscale variability (Viglione et al., 2018; Balwada et al., 2018; Dove et al., 2021, 2022; du Plessis et al., 2019) but also to non-local processes, such as sea ice melt, that influence upper ocean stratification.

2. Data and Methods

2.1. Ocean Glider Data

Two Seagliders carried out meridional transects across the southern Drake Passage from 10 May to 20 August 2016 as part of the Changes in Stratification at the Antarctic Peninsula (ChinStrAP-2) field program (Figure 1). The gliders were profiled in a V-shaped vertical pattern to a maximum depth of 1,000 m, collecting temperature, salinity, and dissolved oxygen concentration data using a SeaBird unpumped CT-Sail and an Aanderaa optode. Optical backscatter at 532 nm was additionally measured to 300 m in the first third of the deployment (10 May–10 June) using a WET Labs ECO puck. Although two gliders were deployed in the field study, analysis from one glider (SG537) is shown here; characteristics are similar between the gliders, as seen in Figure 2 and Figure S1 in Supporting Information S1. The mean separation between glider surfacings at the start and end of dives was 4.6 km (Figure 1a) with a standard deviation of 2.1 km.

The raw glider data were processed using the GliderTools toolbox (Gregor et al., 2019). The data were then mapped onto a regular grid with 5 m vertical spacing and 2.5 km horizontal spacing. The processing and gridding of the glider data are described in full in Text S1 in Supporting Information S1. In this study, we discuss the two northward transects collected by one of the gliders; we term these the "June" transect (spanning 18 May–6 June) and the "July" transect (spanning 8 July–23 July; Figure 1b). Data were processed using the Gibbs Seawater Toolbox (McDougall & Barker, 2011) and the EOS-80 neutral density package (Jackett & McDougall, 1997); we use conservative temperature (Θ), absolute salinity (S_A), and neutral density (γ^n), unless otherwise noted. Mixed layer depths (MLDs) were calculated with a density difference criterion of $\Delta\sigma_0 = 0.125$ kg m^{-3} from the surface (Monterey & Levitus, 1997). Apparent oxygen utilization (AOU) is a tracer, with units of concentration, that removes the temperature dependence of oxygen saturation, and is defined $AOU \equiv \left[O_2^{sat}\right] - [O_2]$ (Ito et al., 2004). Low AOU values are used as a proxy for recent ventilation (Dove et al., 2022; Llort et al., 2018), as respiration in the ocean interior is an oxygen sink.

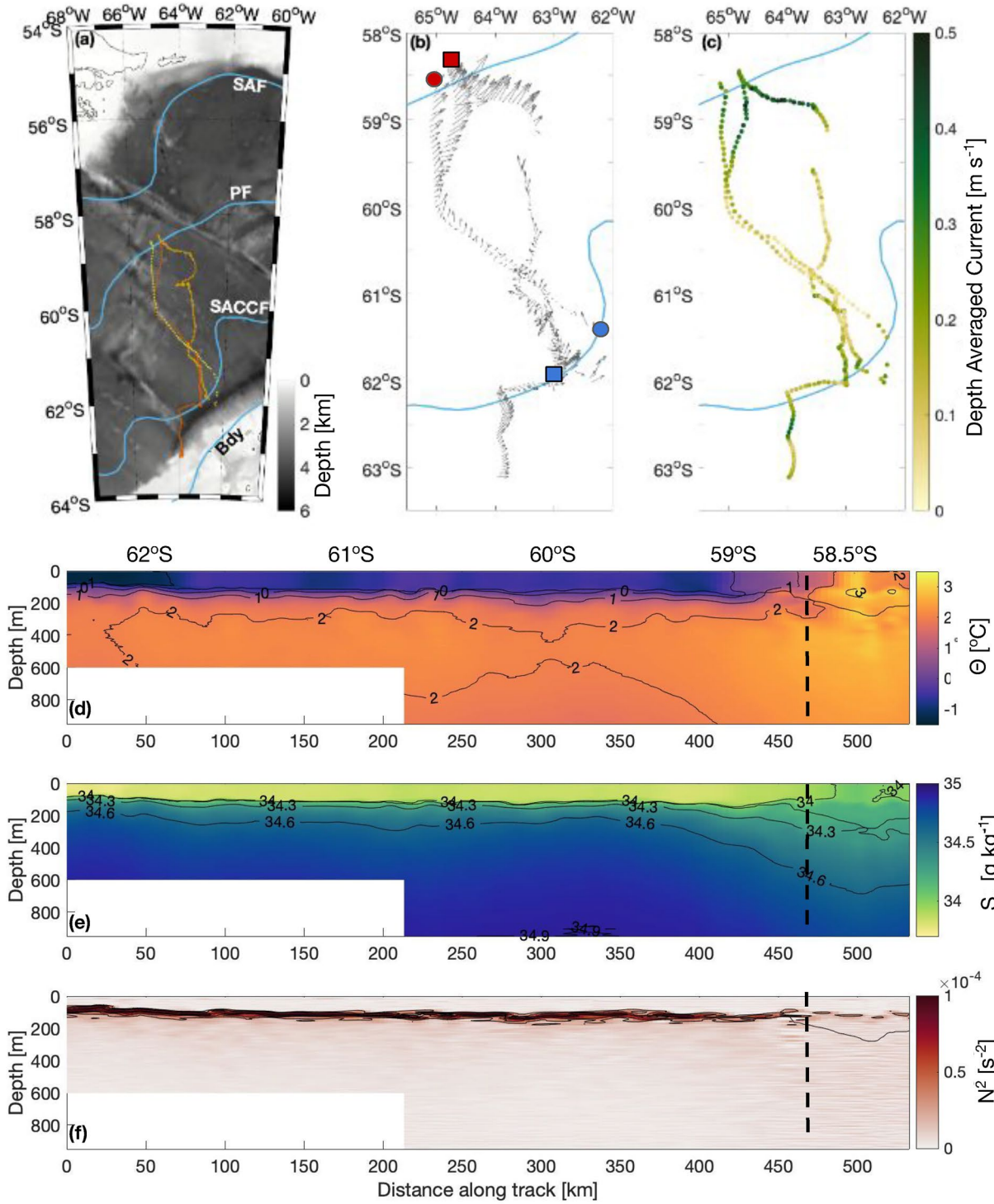

Figure 1. (a) Map of the ChinStrAP2 study region. Individual glider surfacing locations are plotted as dots over ETOPO bathymetry, with red, orange, and yellow distinguishing separate transects. Fronts derived from AVISO altimetry and using the definitions of Kim and Orsi (2014) are plotted in blue and labeled: Subantarctic Front (SAF), Polar Front (PF), Southern ACC Front (SACCF), Southern Boundary (Bdy). (b) Quiver plot of depth-averaged current (to 1,000 m) derived from the glider path. Starting points of the transects discussed are denoted in blue with ending points in red, with the June transect marked with squares and July transect marked with circles. (c) Depth-averaged current speed. Glider data from the June transect, objectively mapped in pressure-distance space, showing (d) conservative temperature (Θ), (e) absolute salinity (S_A), and (f) vertical stratification (N^2). Dashed lines indicate PF crossing.

2.2. Mixing Length Theory (L_{mix})

Ferrari and Nikurashin (2010) argued that mean flows can suppress lateral mixing by advecting tracers away from eddy-rich regions before stirring can cascade tracer variance to smaller scales. This effect was later quantified from observations (Naveira Garabato et al., 2011) using the mixing length theory that describes a characteristic length scale over which a fluid parcel can move before exchanging properties with the background fluid. This analysis was focused on hydrographic sections across major fronts of the ACC at mesoscale resolution (~50 km station separation). Since waters of the southern Drake Passage are salinity stratified, mixing lengths are calculated using conservative temperature, Θ, following:

$$L_{mix} = \frac{\Theta_{rms}}{\nabla_n \Theta_m}. \quad (1)$$

First, Θ is mapped from objectively interpolated pressure coordinates to neutral density space using an interval of $\Delta\gamma_n = 0.02$ kg m^{-3}. A horizontal running mean at 25 km scales produces a low-pass spatial-mean temperature field, Θ_m, from which a large-scale temperature gradient along neutral surfaces, $\nabla_n\Theta_m$, is calculated. Temperature anomalies are defined as deviations from this mean per gridded profile. The first baroclinic Rossby deformation radius at 60°S is ~20 km (Chelton et al., 1998), so this averaging provides a "mesoscale" mean field. The temperature root mean square, Θ_{rms}, is calculated as the standard deviation of temperature anomalies with a running mean of 5 km. This approach differs slightly from Naveira Garabato et al. (2011), which used both a temporal and spatial mean. Θ_{rms} along each transect provide a realization of the variability at the submesoscale. Using average values from the mixed layer, the mixed layer Rossby deformation radius ($NH_{ml}f^{-1}$) is 3.4 km, suggesting 5 km averaging at least partially captures properties at submesoscale.

The mixing length can be combined with an eddy velocity, U_e, and a correlation coefficient, c_e, to estimate an eddy diffusivity, κ, using the relationship:

$$\kappa = c_e U_e L_{mix}. \quad (2)$$

An eddy velocity scale was not calculated from the glider data, but an estimate of eddy kinetic energy (EKE) can be determined from satellite-derived surface geostrophic velocity. In June and July 2016, the time-mean EKE in Drake Passage was 0.01 m^2 s^{-2}, or $U_e \approx EKE^{1/2} = 0.1$ m s^{-1}, with no significant change over the study period. Following Naveira Garabato et al. (2011), we apply $c_e = 0.16$.

2.3. Characterization of the Study Site

Each glider transect traversed the Southern ACC Front and the PF, defined using both hydrographic definitions (Orsi et al., 1995) and ADT contours of −98.5 and −61 cm, respectively (Kim & Orsi, 2014). The ADT contour definitions match the crossing of the PF by the glider as defined by hydrography, the northernmost extent of 2°C water at 200 m (Figure S2 in Supporting Information S1). Velocity sections were constructed by calculating the geostrophic shear from the glider density field and then referencing this velocity to the glider's depth-averaged current (DAC). DAC is calculated from glider trajectories using the difference between the glider's expected and the actual surface location at the end of each profile and applying a glider flight model. The maximum observed geostrophic velocity of the PF was similar during the June crossing (49 cm s^{-1}) and the July crossing (42 cm s^{-1}; Figures 1b and 1c), similar to velocities described in the literature (Firing et al., 2011; Foppert et al., 2016). The geostrophic component of the velocity field is resolved in the direction perpendicular to the glider path and therefore the inferred intensity of the PF is dependent on the angle at which the glider crosses the front. However, the angles at which the glider crossed the PF differed by only ~10% between the crossings.

During the glider deployment, the mean surface heat flux in Drake Passage from the ERA5 reanalysis European Center for Medium-Range Weather Forecasts was −50 W m^{-2}, (over the box bounded by 55°S, 65°S and 60°W, 70°W), consistent with wintertime heat flux in Drake Passage (Stephenson Jr. et al., 2012). The average wind speed over this time period was 10.1 m s^{-1} with maximum winds reaching 21.4 m s^{-1} (Figure S3 in Supporting Information S1). The winds are predominantly westerly, with a westerly wind stress of 0.1 N m^{-2} averaged over the deployment period.

3. Results

3.1. Mixed Layer Properties

The PF marks a transition between salinity-stratified (south of the PF) and temperature-stratified (north of the PF) regions of the Southern Ocean (Stewart & Haine, 2016). The PF also marks a transition in upper ocean mixed layer variability. South of the PF, the mixed layer in 2016 was relatively cold and fresh, bounded below by a strong pycnocline (Figures 1d and 1e). This freshwater lens largely suppressed variations in the MLD: the mean and standard deviation of the MLD was 105.4 ± 13.0 m. On approaching the PF, the mixed layer deepened and the stratification at the base of the mixed layer weakened (Figure 1f). During the June crossing of the PF, the maximum MLD was 199 m. The maximum MLD deepened to 386 m during the July crossing (Figure S4 in Supporting Information S1).

The freshwater lens south of the PF had an average temperature of −0.79°C and an average salinity of 33.67 g kg^{-1}. This temperature value is consistent with the average value measured by Expendable Bathythermograph transects across Drake Passage in winter (Meredith et al., 2011; Sprintall, 2003). The observed fresh and cold values are consistent with sea ice melt (Meredith et al., 2011), which is notable because sea ice does not occupy this region

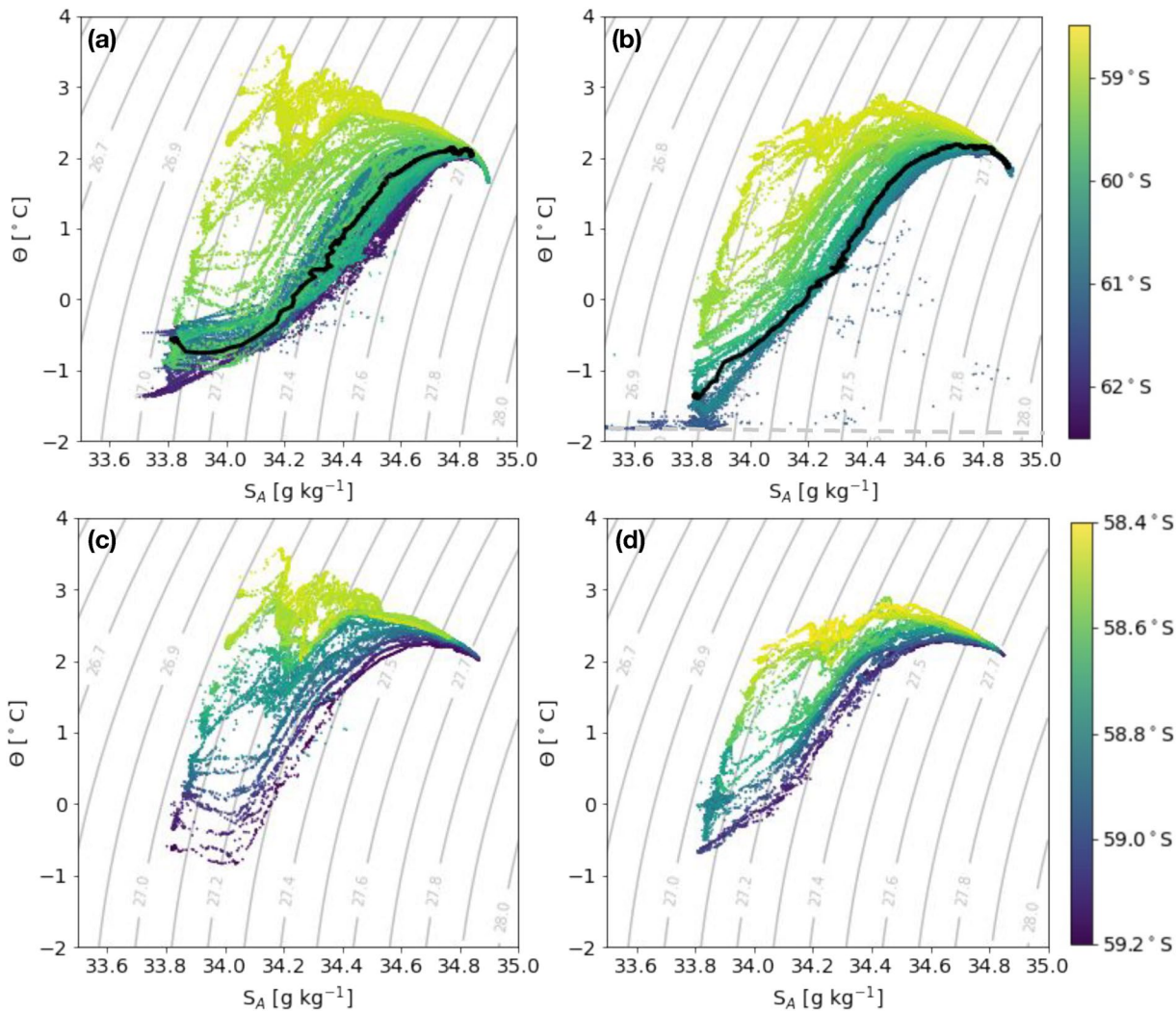

Figure 2. Conservative temperature (Θ)-absolute salinity (S_A) diagrams for the (left) June northward transect and (right) July northward transect. Points are colored by the latitude at which they were collected. (a),(b) show data for the entire transect, with black lines indicating representative glider profiles south of the polar front (PF); (c),(d) show data only in the region immediately surrounding the PF (approximately 1° latitude). Dashed line on (b) indicates the freezing point of seawater. Note the change in color scale range between upper and lower panels.

of Drake Passage. Instead, this layer was likely sourced remotely, and based on the regional circulation, advected from the West Antarctic Peninsula and the Bellingshausen Sea.

3.2. Fine-Scale Structure of the Polar Front

A striking feature of the glider-derived high resolution hydrographic transects is the water mass structure reflected in temperature and salinity properties (Figure 2). The major fronts of the ACC support abrupt changes in hydrographic properties (Orsi et al., 1995) that can be diagnosed as gaps or low concentrations of observations in Θ/S_A space when considering data with uniform horizontal sampling. Naveira Garabato et al. (2011) highlighted these distinctive, well-defined clusters of Θ/S_A curves at mesoscale resolution. Fronts appear as gaps in Θ/S_A space, while profiles within each inter-frontal zone fall within a narrow range of properties.

In Θ/S_A space, there are two clear regimes along the glider transects. South of the PF, the Θ/S_A profiles largely fall onto a single curve that has limited variability throughout the deployment (black lines in Figures 2a and 2b). Additionally, all of the profiles converge to the same temperature and salinity (1.6°C and 34.9 g kg^{-1}) at the base of the thermocline that represents the subsurface reservoir of Upper Circumpolar Deep Water.

In contrast, surface waters at the PF span a larger range of Θ and S_A values (Figures 2c and 2d). The "PF crossing" waters are from glider profiles within 50 km of the PF for each transect. The distribution of Θ/S_A properties in the surface mixed layer along 27.05 kg m^{-3} is more continuous than the waters in the transition layer located between 27.05 and 27.25 kg m^{-3}. The Θ/S_A properties in this transition layer group into discrete "families" with distinct Θ/S_A properties (Figures 2c and 2d). Reminiscent of the analysis of Θ/S_A at the mesoscale, gaps in Θ/S_A space over this narrow band of ∼1° of latitude are indicative of submesoscale fronts that result in the propagation of discrete hydrographic properties below the base of the mixed layer, consistent with the important role of filaments in ventilation (Balwada et al., 2018; Dove et al., 2021; Freilich & Mahadevan, 2021).

3.3. Mean-Flow Suppression at the Polar Front

We re-visit the approach of Naveira Garabato et al. (2011) with the ability to assess whether smaller-scale frontal structure impacts mixing properties. Across the June and July transects, the hydrographic signature of the PF is located just north of 59°S (dashed black line in Figures 3a and 3b), consistent with a strongly elevated $\nabla_n\Theta_m$ (Figures 3c and 3d). The strong temperature gradient combines with mesoscale and submesoscale stirring to enhance temperature variance (Θ_{rms}) in the PF (Figures 3e and 3f). The distribution of Θ_{rms} captures smaller-scale variability, highlighting intermittent patches of enhanced variance south of the PF. Enhanced tracer variance found in density classes below the mixed layer south of the PF may represent tracer variance generated within the PF advecting southward along the upwelling limb of the overturning circulation and is a topic of future work.

The estimated values of the mixing length, L_{mix}, range from 0 to >100 km (Figures 3g and 3h). Similar to property distributions in Θ/S_A space, there are two regimes. South of the PF, L_{mix} reaches its largest value. There is potentially a shift from large values of L_{mix} to smaller values from the June to July transects, although this limited temporal resolution makes it difficult to infer whether this is related to a seasonal evolution or a shift in the mesoscale background properties. In contrast, in both transects, L_{mix} is suppressed at the PF, with the smallest values confined to a region <50 km wide. The vertically-averaged mixing length at the PF is L_{mix} = 11 km and L_{mix} = 10 km in June and July, respectively. These values are consistent with the findings of Naveira Garabato et al. (2011) from non-winter months and Foppert et al. (2016) from a full year but augment these studies by directly resolving the inferred scale of the mixing length. From multiple crossings of the PF, our results imply that the PF acts as a barrier to upper ocean mixing, not only at mesoscales but also at submesoscales, in wintertime Drake Passage. Finally, using (2) we estimate κ at the PF as ≈170 m^2 s^{-1}, a value that corroborates that mesoscale stirring is not efficient at the PF.

3.4. Biogeochemical Signatures of Ventilation

The distribution of AOU in Drake Passage also supports spatial variations in ventilation. The June transect, representative of both transects, shows that low-AOU waters, indicative of recent ventilation, are confined to the mixed layer south of the PF. At the PF, the combination of a weakened vertical stratification and tilted isopycnals

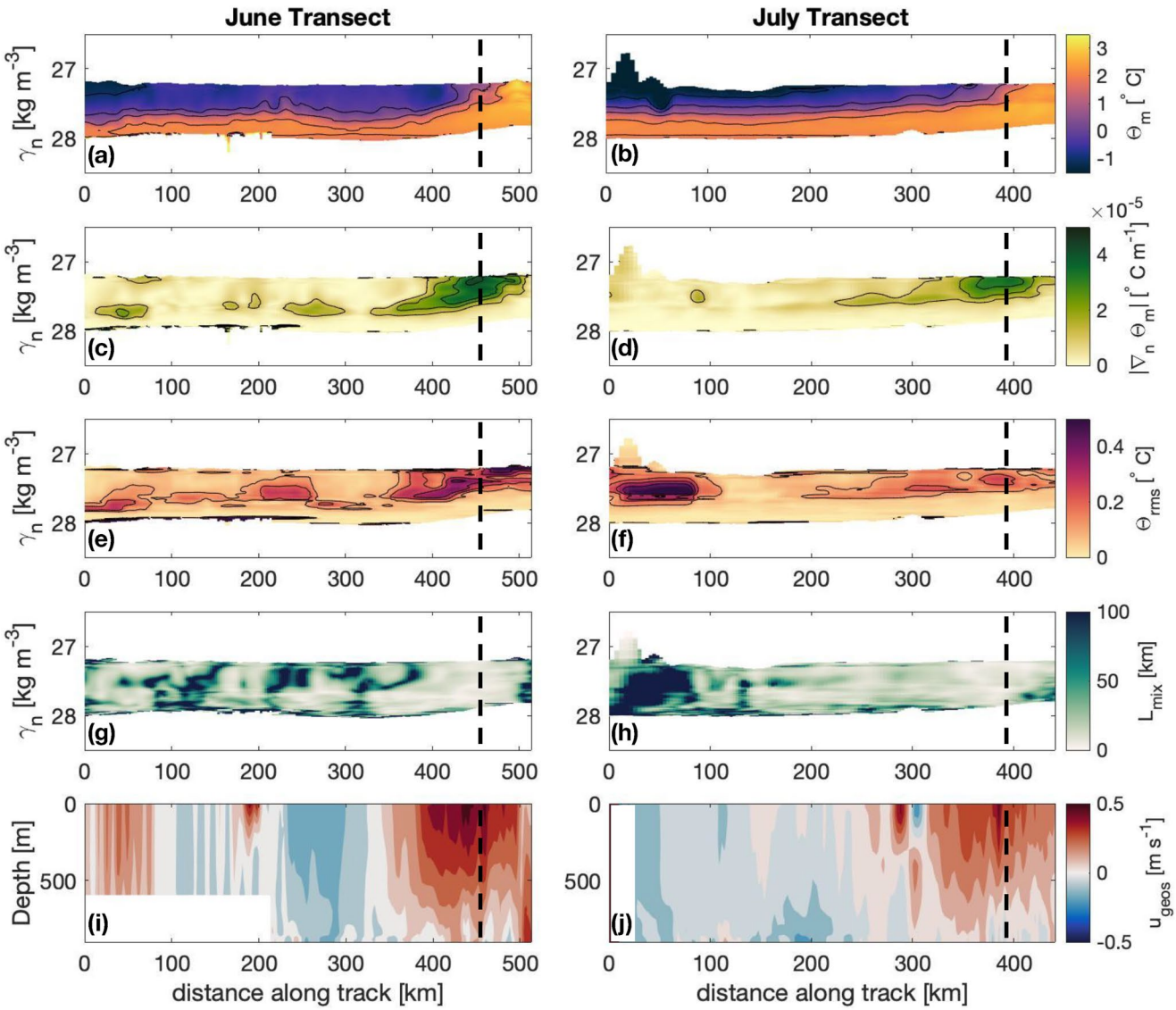

Figure 3. Mixing characteristics along two northbound glider transects spanning southern Drake Passage. Panels (a)–(h) are plotted in distance-neutral density space, panels (i),(j) are plotted in distance-pressure space. Left-hand panels (a,c,e,g,i) show observations from the June transect; right-hand panels (b,d,f,h,j) show observations from the July transect. (a),(b) Smoothed temperature, Θ_m. (c),(d) Large-scale temperature gradient along isoneutral surfaces, $\nabla_n\Theta_m$. (e),(f) Standard deviation of temperature fluctuations, Θ_{rms}. (g),(h) Eddy mixing length, L_{mix}.(i),(j) Geostrophic velocity, U_{geo}. Black dashed lines indicate polar front crossings.

(Figure 4a) allows low-AOU waters to extend over 100 m below the base of the mixed layer. These low-AOU waters penetrate to depth primarily along isopycnals, suggesting a key role for rapid adiabatic advection or stirring in ventilation. These observations are consistent with numerical modeling studies that show that exchange at localized fronts can dominate larger-scale tracer fluxes (Uchida et al., 2019). MLD reaches its maximum extent in July and August in Drake Passage (Pellichero et al., 2017); therefore, we expect any tracer subducted at the PF is unlikely to be re-entrained to the mixed layer.

The high-resolution sampling capabilities of the glider permit an analysis of tracer variance at submesoscale resolution. The transition between a near-continuous distribution of Θ/S_A properties in the mixed layer to a discrete collection of Θ/S_A "families" in the transition layer provides compelling evidence that water is ventilated from the surface into the interior in small-scale filaments (Figures 2c and 2d). Specifically, the filamentary structure occurs in the same localized region near the PF where low-AOU waters penetrate to depth along isopycnals (Figure 4a), suggesting submesoscale processes contribute to the ventilation. We acknowledge that this venti-

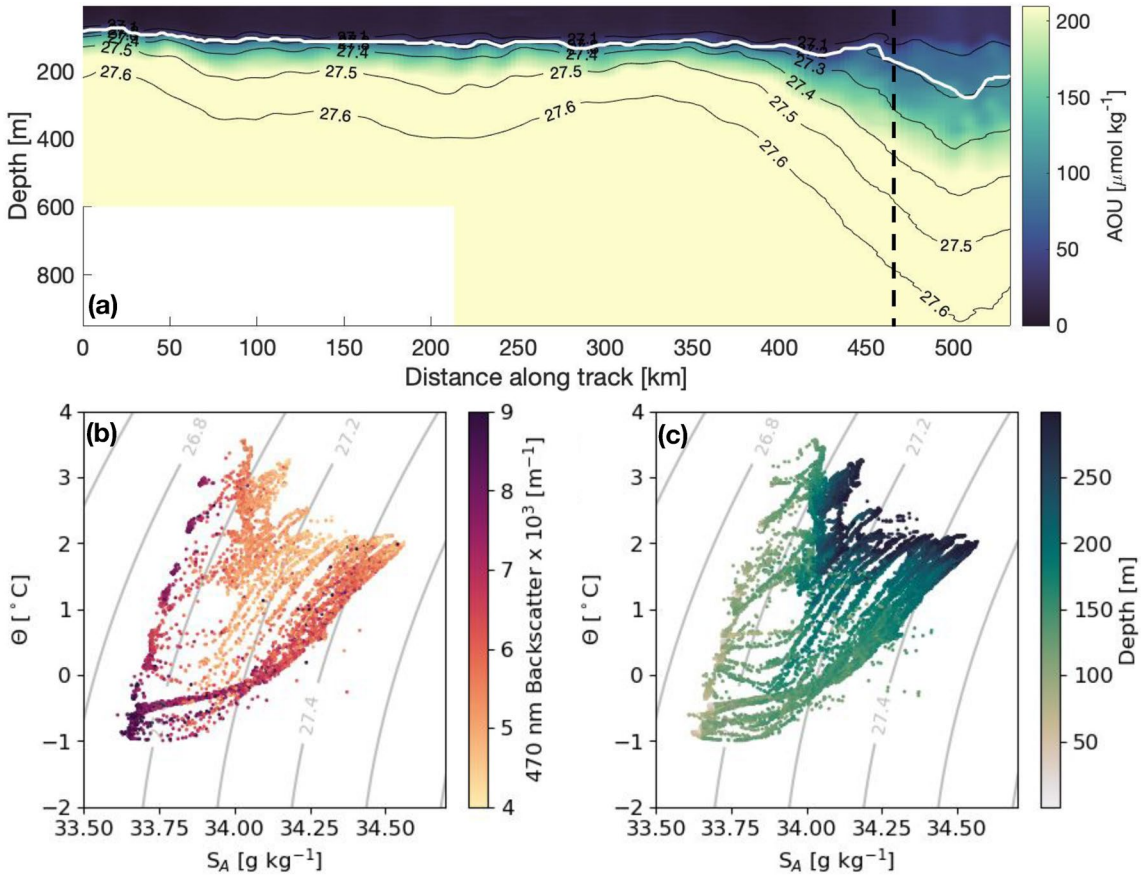

Figure 4. Biogeochemical signatures from the Polar Front. (a) Distance-depth section of apparent oxygen utilization (AOU) for the June transect. Gray lines indicate isopycnals and the white line is the mixed layer depth. Θ/S_A diagrams for (b) 532 nm optical backscatter and (c) depth. Optical backscatter was only measured to 300 m depth.

lation may occur upstream of the glider observations, and there are fundamental limitations in documenting three-dimensional ventilation processes from individual transects.

Along-isopycnal variations in optical backscatter suggest a pathway for the transport of particulate organic carbon from the surface to the interior ocean. Waters with high particulate content from the southern edge of the PF are preferentially found at depth within a density range that occupies a relatively small fraction of the surface water occupied by the gliders (Figures 4b and 4c). This is consistent with process-modeling studies that show subduction of near-surface waters is typically located along the dense side of fronts, which can further localize ventilated waters to mesoscale or smaller regions (Freilich & Mahadevan, 2021).

4. Discussion

The Southern Ocean has traditionally been identified as a region preconditioned for strong submesoscale activity due to strong surface wind and buoyancy forcing and a weak vertical stratification (Gille et al., 2022; Su et al., 2018). Yet, despite strong wind stress and surface cooling (Figure S3 in Supporting Information S1), the glider sections presented here show limited signatures of submesoscale variability and ventilation throughout the southern Drake Passage. The fresh and cold mixed layer water properties found south of the PF indicate that non-local processes—for example, the advection of waters influenced by sea ice melt from the West Antarctic Peninsula and Bellingshausen Sea—influence surface-interior exchange far from the melt location. In contrast, both tracer distributions (Figure 2) and tracer variance (L_{mix} calculation in Figure 3) suggest local small-scale, or submesocale, control on ventilation at the PF.

This work builds on the study of Naveira Garabato et al. (2011) in two important ways: first, our analysis was carried out using higher-resolution data (glider- vs. ship-based), and second, their analysis was carried out during the summer and autumn months. The calculated mixing lengths, in regions where mean-flow suppression both is and is not active, have similar magnitudes, but the spatial scales of variability in Naveira Garabato et al. (2011) are much broader. Direct resolution of the suppressed mixing lengths of $O(10)$ km provides confidence that suppression of eddy stirring is strong in the upper and intermediate layers within the PF, and may even contribute to setting the small-scale distribution of water mass properties (Figure 2). Larger values of L_{mix} and weak isopycnal gradients are consistent with homogenization south of the PF, which may suppress the generation of strong submesoscale fronts.

Sallée et al. (2012) highlighted all of Drake Passage as a key site of mode water formation and tracer ventilation, based on coarsely resolved in situ and remote sensing data. In recent years, higher resolution models and observations have indicated significant heterogeneity in surface properties, influencing ventilation and air–sea fluxes, in regions as small as Drake Passage. The need to resolve and mechanistically understand these variations is particularly acute in Drake Passage since it is the principal location from which the Surface Ocean CO_2 Atlas underway pCO_2 data is collected in winter (Bakker et al., 2016). Analysis of Southern Ocean Carbon and Climate Observations and Modeling (SOCCOM) biogeochemical-Argo float data (Gray et al., 2018) found stronger CO_2 outgassing south of the PF than previous estimates. While this discrepancy remains unexplained—in fact, Long et al. (2021) found strong carbon uptake south of 45°S—a potential for bias can arise if the region of weak surface-interior exchange in the southern Drake Passage is extrapolated zonally. More broadly, the observations presented here highlight complications linked to extrapolating local measurements to other regions based purely based on geographical considerations, for example, latitude. While the SOCCOM program has begun to identify regional variations in air–sea exchange (Prend et al., 2022), the abrupt spatial transitions in dynamical regimes that occur in the ACC imply that global estimates of air-sea fluxes will continue to have substantial uncertainties.

5. Conclusions

The ChinStrAP2 field campaign provided a unique dataset comprising several high-resolution transects of Drake Passage collected by ocean gliders in wintertime. These observations have offered new insight into the fine-scale structures of the PF. We find that the PF acts to suppress eddy mixing, even at scales below mesoscale eddies. We also reveal that submesoscale variability, including exchange across the base of the mixed layer, is suppressed south of the PF, even with strong wintertime surface forcing, due to enhanced vertical stratification that occurs due to meltwater water advected into the region from upstream. Ventilation over the study region is restricted to a narrow region (~1° of latitude) near the PF. Here, the stratification weakens, the mixed layers deepen, and small-scale (submesoscale) water masses are found in the mixed layer pycnocline. The sensitivity of ventilation to both large-scale, even remote, processes as well as fine-scale frontal structure, suggests the need for scale-aware and adaptive future observing arrays to constrain Southern Ocean-wide heat, carbon, and nutrient budgets.

Acknowledgments
LAD was financially supported by the Resnick Sustainability Institute and an NSF graduate research fellowship. GAV and AFT were supported by NSF Award OPP-1246460. MMF was supported by the Internal Research and Technology Development program (Earth 2050 project) through the Jet Propulsion Laboratory, California Institute of Technology. TRC was supported by a Resnick Sustainability Institute WAVE summer research fellowship. JS was supported by NSF Awards OPP-1246160 and OCE-1755529. The authors would like to thank the Antarctic Support Contract staff as well as the captains and crews of the ARSV Laurence M. Gould for their support during the deployment and recovery cruises. LAD thanks Zachary K. Erickson for useful discussions while preparing this manuscript. The authors are grateful for the reviews of four reviewers, whose critiques improved the quality of this manuscript.

Data Availability Statement

Seaglider data are archived at the NOAA National Centers for Environmental Information (https://www.ncei.noaa.gov/archive/accession/0276223). Sea level anomaly and surface velocity products were produced and distributed by the Copernicus Marine 360 and Environment Monitoring Service (https://data.marine.copernicus.eu/product/SEALEVEL_GLO_PHY_L4_MY_008_047/description). Estimates of surface forcing fields (wind speed and direction, surface heat fluxes) for Drake Passage were obtained from the ERA5 atmospheric reanalysis from the European Centre for Medium-Range Weather Forecasts (https://cds.climate.copernicus.eu/cdsapp#!/dataset/10.24381/cds.bd0915c6).

References

Abernathey, R. P., Cerovecki, I., Holland, P. R., Newsom, E., Mazloff, M., & Talley, L. D. (2016). Water-mass transformation by sea ice in the upper branch of the Southern Ocean overturning. *Nature Geoscience*, *9*(8), 596–601. https://doi.org/10.1038/ngeo2749

Adams, K. A., Hosegood, P., Taylor, J. R., Sallée, J.-B., Bachman, S., Torres, R., & Stamper, M. (2017). Frontal circulation and submesoscale variability during the formation of a Southern Ocean mesoscale eddy. *Journal of Physical Oceanography*, *47*(7), 1737–1753. https://doi.org/10.1175/jpo-d-16-0266.1

Bachman, S. D., Taylor, J. R., Adams, K. A., & Hosegood, P. J. (2017). Mesoscale and submesoscale effects on mixed layer depth in the Southern Ocean. *Journal of Physical Oceanography*, *47*(9), 2173–2188. https://doi.org/10.1175/jpo-d-17-0034.1

Bakker, D. C. E., Pfeil, B., Landa, C. S., Metzl, N., O'Brien, K. M., Olsen, A., et al. (2016). A multi-decade record of high-quality fCO_2 data in version 3 of the Surface Ocean CO_2 Atlas (SOCAT). *Earth System Science Data*, *8*(2), 383–413.

Balwada, D., Smith, K. S., & Abernathey, R. (2018). Submesoscale vertical velocities enhance tracer subduction in an idealized Antarctic Circumpolar Current. *Geophysical Research Letters*, *45*(18), 9790–9802. https://doi.org/10.1029/2018gl079244

Chapman, C. C., Lea, M.-A., Meyer, A., Sallée, J.-B., & Hindell, M. (2020). Defining Southern Ocean fronts and their influence on biological and physical processes in a changing climate. *Nature Climate Change*, *10*(3), 209–219. https://doi.org/10.1038/s41558-020-0705-4

Chelton, D. B., de Szoeke, R. A., Schlax, M. G., Naggar, K. E., & Siwertz, N. (1998). Geographical variability of the first baroclinic Rossby radius of deformation. *Journal of Physical Oceanography*, *28*(3), 433–460. https://doi.org/10.1175/1520-0485(1998)028⟨0433:GVOTFB⟩2.0.CO;2

Close, S. E., Naveira Garabato, A. C., McDonagh, E. L., King, B. A., Biuw, M., & Boehme, L. (2013). Control of mode and intermediate water mass properties in Drake passage by the Amundsen sea low. *Journal of Climate*, *26*(14), 5102–5123. https://doi.org/10.1175/jcli-d-12-00346.1

Dove, L. A., Balwada, D., Thompson, A. F., & Gray, A. R. (2022). Enhanced ventilation in energetic regions of the Antarctic circumpolar current. *Geophysical Research Letters*, *49*(13), e2021GL097574. https://doi.org/10.1029/2021GL097574

Dove, L. A., Thompson, A. F., Balwada, D., & Gray, A. R. (2021). Observational evidence of ventilation hotspots in the Southern Ocean. *Journal of Geophysical Research: Oceans*, *126*(7), e2021JC017178. https://doi.org/10.1029/2021JC017178

du Plessis, M., Swart, S., Ansorge, I. J., & Mahadevan, A. (2017). Submesoscale processes promote seasonal restratification in the Subantarctic Ocean. *Journal of Geophysical Research: Oceans*, *122*(4), 2960–2975. https://doi.org/10.1002/2016jc012494

du Plessis, M., Swart, S., Ansorge, I. J., Mahadevan, A., & Thompson, A. F. (2019). Southern Ocean seasonal restratification delayed by submesoscale wind–front interactions. *Journal of Physical Oceanography*, *49*(4), 1035–1053. https://doi.org/10.1175/JPO-D-18-0136.1

Ferrari, R., Jansen, M. F., Adkins, J. F., Burke, A., Stewart, A. L., & Thompson, A. F. (2014). Antarctic sea ice control on ocean circulation in present and glacial climates. *Proceedings of the National Academy of Sciences (USA)*, *111*(24), 8753–8758. https://doi.org/10.1073/pnas.1323922111

Ferrari, R., & Nikurashin, M. (2010). Suppression of eddy diffusivity across jets in the Southern Ocean. *Journal of Physical Oceanography*, *40*(7), 1501–1519. https://doi.org/10.1175/2010jpo4278.1

Firing, Y. L., Chereskin, T. K., & Mazloff, M. R. (2011). Vertical structure and transport of the Antarctic Circumpolar Current in Drake Passage from direct velocity observations. *Journal of Geophysical Research*, *116*(C8), C08015. https://doi.org/10.1029/2011JC006999

Foppert, A., Donohue, K. A., & Watts, D. R. (2016). The polar front in Drake passage: A composite-mean stream-coordinate view. *Journal of Geophysical Research: Oceans*, *121*(3), 1771–1788. https://doi.org/10.1002/2015JC011333

Freilich, M., & Mahadevan, A. (2021). Coherent pathways for subduction from the surface mixed layer at ocean fronts. *Journal of Geophysical Research: Oceans*, *126*(5), e2020JC017042. https://doi.org/10.1029/2020JC017042

Frölicher, T. L., Sarmiento, J. L., Paynter, D. J., Dunne, J. P., Krasting, J. P., & Winton, M. (2015). Dominance of the Southern Ocean in anthropogenic carbon and heat uptake in CMIP5 models. *Journal of Climate*, *28*(2), 862–886. https://doi.org/10.1175/JCLI-D-14-00117.1

Giddy, I., Swart, S., Plessis, M. d., Thompson, A. F., & Nicholson, S.-A. (2021). Stirring of sea-ice meltwater enhances submesoscale fronts in the Southern Ocean. *Journal of Geophysical Research: Oceans*, *126*(4), e2020JC016814. https://doi.org/10.1029/2020JC016814

Gille, S. T., Sheen, K. L., Swart, S., & Thompson, A. F. (2022). Chapter 12 - mixing in the Southern Ocean. In M. Meredith & A. Naveira Garabato (Eds.), *ocean mixing* (pp. 301–327). Elsevier. https://doi.org/10.1016/B978-0-12-821512-8.00019-0

Gray, A. R., Johnson, K. S., Bushinsky, S. M., Riser, S. C., Russell, J. L., Talley, L. D., et al. (2018). Autonomous biogeochemical floats detect significant carbon dioxide outgassing in the high-latitude Southern Ocean. *Geophysical Research Letters*, *45*(17), 9049–9057. https://doi.org/10.1029/2018GL078013

Gregor, L., Ryan-Keogh, T. J., Nicholson, S.-A., du Plessis, M., Giddy, I., & Swart, S. (2019). GliderTools: A Python toolbox for processing underwater glider data. *Frontiers in Marine Science*, *6*. Retrieved 2022-11-12, from. https://doi.org/10.3389/fmars.2019.00738

Ito, T., Follows, M. J., & Boyle, E. A. (2004). Is AOU a good measure of respiration in the oceans? *Geophysical Research Letters*, *31*(17). https://doi.org/10.1029/2004GL020900

Jackett, D. R., & McDougall, T. J. (1997). A neutral density variable for the world's oceans. *Journal of Physical Oceanography*, *27*(2), 237–263. https://doi.org/10.1175/1520-0485(1997)027<0237:andvft>2.0.co;2

Kim, Y. S., & Orsi, A. H. (2014). On the variability of Antarctic Circumpolar Current fronts inferred from 1992–2011 altimetry. *Journal of Physical Oceanography*, *44*(12), 3054–3071. https://doi.org/10.1175/jpo-d-13-0217.1

Klein, P., & Lapeyre, G. (2009). The oceanic vertical pump induced by mesoscale and submesoscale turbulence. *Annu. Rev. Mar. Sci.*, *1*, 351–375. https://doi.org/10.1146/annurev.marine.010908.163704

Klocker, A., Ferrari, R., & LaCasce, J. H. (2012). Estimating suppression of eddy mixing by mean flows. *Journal of Physical Oceanography*, *42*(9), 1566–1576. https://doi.org/10.1175/jpo-d-11-0205.1

Landschützer, P., Gruber, N., Haumann, F. A., Rödenbeck, C., Bakker, D. C. E., Heuven, S. v., et al. (2015). The reinvigoration of the Southern Ocean carbon sink. *Science*, *349*(6253), 1221–1224. https://doi.org/10.1126/science.aab2620

Llort, J., Langlais, C., Matear, R., Moreau, S., Lenton, A., & Strutton, P. G. (2018). Evaluating southern Ocean Carbon eddy-pump from biogeochemical-Argo floats. *Journal of Geophysical Research: Oceans*, *123*(2), 971–984. https://doi.org/10.1002/2017JC012861

Long, M. C., Stephens, B. B., McKain, K., Sweeney, C., Keeling, R. F., Kort, E. A., et al. (2021). Strong Southern Ocean carbon uptake evident in airborne observations. *Science*, *374*(6572), 1275–1280. https://doi.org/10.1126/science.abi4355

McDougall, T. J., & Barker, P. M. (2011). Getting started with TEOS-10 and the Gibbs Seawater (GSW) oceanographic toolbox. *SCOR/IAPSO WG*, *127*, 1–28.

Meredith, M. P., Woodworth, P. L., Chereskin, T. K., Marshall, D. P., Allison, L. C., Bigg, G. R., et al. (2011). Sustained monitoring of the Southern Ocean at Drake passage: Past achievements and future priorities. *Reviews of Geophysics*, *49*(4). https://doi.org/10.1029/2010RG000348

Monterey, G. I., & Levitus, S. (1997). *Seasonal variability of mixed layer depth for the world ocean*. US Department of Commerce, National Oceanic and Atmospheric Administration, National Environmental Satellite, Data, and Information Service.

Morrison, A. K., Waugh, D. W., Hogg, A. M., Jones, D. C., & Abernathey, R. P. (2022). Ventilation of the Southern Ocean pycnocline. *Annual Review of Marine Science*, *14*(1), 405–430. https://doi.org/10.1146/annurev-marine-010419-011012

Naveira Garabato, A. C., Ferrari, R., & Polzin, K. L. (2011). Eddy stirring in the southern ocean. *Journal of Geophysical Research*, *116*(C9), C09019. https://doi.org/10.1029/2010jc006818

Naveira Garabato, A. C., Jullion, L., Stevens, D. P., Heywood, K. J., & King, B. A. (2009). Variability of Subantarctic mode water and Antarctic intermediate water in the Drake passage during the late-twentieth and early-twenty-first centuries. *Journal of Climate*, *22*(13), 3661–3688. https://doi.org/10.1175/2009jcli2621.1

Orsi, A. H., Whitworth, T., & Nowlin, W. D. (1995). On the meridional extent and fronts of the Antarctic Circumpolar Current. *Deep-Sea Research Part I*, *42*(5), 641–673. https://doi.org/10.1016/0967-0637(95)00021-w

Pellichero, V., Sallée, J.-B., Chapman, C. C., & Downes, S. M. (2018). The southern ocean meridional overturning in the sea-ice sector is driven by freshwater fluxes. *Nature Communications*, *9*(1), 1789. https://doi.org/10.1038/s41467-018-04101-2

Pellichero, V., Sallée, J.-B., Schmidtko, S., Roquet, F., & Charrassin, J.-B. (2017). The ocean mixed layer under Southern Ocean sea-ice: Seasonal cycle and forcing. *Journal of Geophysical Research-Oceans*, *122*(2), 1608–1633. https://doi.org/10.1002/2016jc011970

Prend, C. J., Gray, A. R., Talley, L. D., Gille, S. T., Haumann, F. A., Johnson, K. S., et al. (2022). Indo-Pacific sector dominates Southern Ocean Carbon outgassing. *Global Biogeochemical Cycles*, *36*(7), e2021GB007226. https://doi.org/10.1029/2021GB007226

Rosso, I., Hogg, A. M., Strutton, P. G., Kiss, A. E., Matear, R., Klocker, A., & van Sebille, E. (2014). Vertical transport in the ocean due to sub-mesoscale structures: Impacts in the Kerguelen region. *Ocean Modelling*, *80*, 10–23. https://doi.org/10.1016/j.ocemod.2014.05.001

Sallée, J.-B., Matear, R. J., Rintoul, S. R., & Lenton, A. (2012). Localized subduction of anthropogenic carbon dioxide in the Southern Hemisphere oceans. *Nature Geoscience*, *5*(8), 579–584. https://doi.org/10.1038/ngeo1523

Sallée, J.-B., Speer, K. G., & Rintoul, S. R. (2010). Zonally asymmetric response of the Southern Ocean mixed-layer depth to the southern annular mode. *Nature Geoscience*, *3*(4), 273–279. https://doi.org/10.1038/ngeo812

Speer, K., Rintoul, S. R., & Sloyan, B. (2000). The diabatic deacon cell. *Journal of Physical Oceanography*, *30*(12), 3212–3222. https://doi.org/10.1175/1520-0485(2000)030<3212:tddc>2.0.co;2

Sprintall, J. (2003). Seasonal to interannual upper-ocean variability in the Drake Passage. *Journal of Marine Researc*h, *61*(1), 27–57. https://doi.org/10.1357/002224003321586408

Stephenson, G. R., Jr., Gille, S. T., & Sprintall, J. (2012). Seasonal variability of upper ocean heat content in Drake Passage. *Journal of Geophysical Research*, *117*(C4). https://doi.org/10.1029/2011JC007772

Stewart, K. D., & Haine, T. W. N. (2016). Thermobaricity in the transition zones between Alpha and Beta oceans. *Journal of Physical Oceanography*, *46*(6), 1805–1821. https://doi.org/10.1175/JPO-D-16-0017.1

Stukel, M. R., Aluwihare, L. I., Barbeau, K. A., Chekalyuk, A. M., Goericke, R., Miller, A. J., et al. (2017). Mesoscale ocean fronts enhance carbon export due to gravitational sinking and subduction. *Proceedings of the National Academy of Sciences*, *114*(6), 1252–1257. https://doi.org/10.1073/pnas.1609435114

Su, Z., Wang, J., Klein, P., Thompson, A. F., & Menemenlis, D. (2018). Ocean submesoscales as a key component of the global heat budget. *Nature Communications*, *9*(1), 775. https://doi.org/10.1038/s41467-018-02983-w

Sutton, A. J., Williams, N. L., & Tilbrook, B. (2021). Constraining Southern Ocean CO_2 flux uncertainty using uncrewed surface vehicle observations. *Geophysical Research Letters*, *48*(3), e2020GL091748. https://doi.org/10.1029/2020GL091748

Takahashi, T., Sutherland, S. C., Wanninkhof, R., Sweeney, C., Feely, R. A., Chipman, D. W., et al. (2009). Climatological mean and decadal change in surface ocean pCO_2, and net sea-air CO_2 flux over the global oceans. *Deep-Sea Research Part II*, *56*(8), 554–577. https://doi.org/10.1016/j.dsr2.2008.12.009

Takahashi, T., Sweeney, C., Hales, B., Chipman, D. W., Newberger, T., Goddard, J. G., et al. (2012). The changing carbon cycle in the Southern Ocean. *Oceanography*, *25*(3), 26–37. https://doi.org/10.5670/oceanog.2012.71

Thompson, A. F., & Sallée, J.-B. (2012). Jets and topography: Jet transitions and the impact on transport in the Antarctic Circumpolar Current. *Journal of Physical Oceanography*, *42*(6), 956–972. https://doi.org/10.1175/jpo-d-11-0135.1

Uchida, T., Balwada, D., Abernathey, R., McKinley, G., Smith, S., & Lévy, M. (2019). The contribution of submesoscale over mesoscale eddy iron transport in the open Southern Ocean. *Journal of Advances in Modeling Earth Systems*, *11*(12), 3934–3958. https://doi.org/10.1029/2019MS001805

Viglione, G. A., Thompson, A. F., Sprintall, J., Flexas, M. M., & Swart, S. (2018). Abrupt transitions in submesoscale structure in Southern Drake Passage: Glider observations and model results. *Journal of Physical Oceanography*, *48*(9), 2011–2027. https://doi.org/10.1175/jpo-d-17-0192.1

References From the Supporting Information

Bol, R., Henson, S. A., Rumyantseva, A., & Briggs, N. (2018). High-frequency variability of small-particle carbon export flux in the Northeast Atlantic. *Global Biogeochemical Cycles*, *32*(12), 1803–1814. https://doi.org/10.1029/2018GB005963

Briggs, N., Perry, M. J., Cetinić, I., Lee, C., D'Asaro, E., Gray, A. M., & Rehm, E. (2011). High-resolution observations of aggregate flux during a sub-polar North Atlantic spring bloom. *Deep Sea Research Part I: Oceanographic Research Papers*, *58*(10), 1031–1039. https://doi.org/10.1016/j.dsr.2011.07.007

Vaillancourt, R. D., Brown, C. W., Guillard, R. R. L., & Balch, W. M. (2004). Light backscattering properties of marine phytoplankton: Relationships to cell size, chemical composition and taxonomy. *Journal of Plankton Research*, *26*(2), 191–212. https://doi.org/10.1093/plankt/fbh012

Zhang, X., Hu, L., & He, M.-X. (2009). Scattering by pure seawater: Effect of salinity. *Optics Express*, *17*(7), 5698–5710. https://doi.org/10.1364/OE.17.005698